Vibrational behavior of sandwich structures overloaded by fractal distribution of masses

Jérémie Derré, Frank Simon

▶ **To cite this version:**

Jérémie Derré, Frank Simon. Vibrational behavior of sandwich structures overloaded by fractal distribution of masses. Proceedings of meetings on acoustics, 2017, Acoustics '17 Boston 173rd Meeting of Acoustical Society of America and 8th Forum Acusticum, 30, pp.065012. 10.1121/2.0000602 . hal-01716272

HAL Id: hal-01716272
https://hal.science/hal-01716272

Submitted on 23 Feb 2018

HAL is a multi-disciplinary open access archive for the deposit and dissemination of scientific research documents, whether they are published or not. The documents may come from teaching and research institutions in France or abroad, or from public or private research centers.

L'archive ouverte pluridisciplinaire **HAL**, est destinée au dépôt et à la diffusion de documents scientifiques de niveau recherche, publiés ou non, émanant des établissements d'enseignement et de recherche français ou étrangers, des laboratoires publics ou privés.

Proceedings of Meetings on Acoustics

Vibrational behavior of sandwich structures overloaded by fractal distribution of masses

--Manuscript Draft--

Manuscript Number:	
Full Title:	Vibrational behavior of sandwich structures overloaded by fractal distribution of masses
Article Type:	ASA Meeting Paper
Corresponding Author:	Jérémie Derré ONERA Toulouse CEDEX 4, Occitanie FRANCE
Order of Authors:	Jérémie Derré
	Frank Simon
Abstract:	This paper presents the modeling and numerical simulations of the vibrational behavior of sandwich panels locally overloaded by a fractal distribution of masses. The structural model hypotheses consist in a homogenized material, which is overloaded by small masses distributed following a fractal pattern. The flat panel is then uniformly discretized and the spatial derivatives operators are approximated using finite differences. The time-harmonic equation is recast into an eigenvalue problem and solved to find natural frequencies and mode shapes. The panel is simply-supported on all of its edges. Simulations of a non-overloaded panel are compared to analytic results in term of wavenumbers and mode shapes. Simulations of fractally overloaded panels exhibit localization phenomena when the inter-mass distance is comparable to half the structural wavelength. The influence of the fractal distribution is investigated through the fractal order, the modal frequencies, and the evolution of the modal density. The material is designed to reduce the structural vibration but also the acoustic radiation generated by the structure. The finite differences model can be used to compute the acoustic radiation of such a structure.
Section/Category:	Structural Acoustics and Vibration

Powered by Editorial Manager® and ProduXion Manager® from Aries Systems Corporation

Manuscript - Author submits - PDF format ONLY

1. INTRODUCTION

For more than fifty years, lightweight composite materials have been widely used within the transport industry, driven by the benefits of mass reduction. To be more specific, in the aerospace industry, sandwich honeycomb core panels have been used for decades within secondary aircraft parts (*e.g.*, trim panels) and more recently as primary parts (Airbus A350-XWB or NHIndustries NH90 for instance, fuselage and structural elements), maximizing the stiffness-to-weight ratio. The weight reduction is however responsible for a decrease in the panel sound transmission loss and a rise in the acoustic radiation (*e.g.*, mass law before the coincidence frequency),[1] which has to be compensated particularly for acoustical safety and comfort. Hence, strategies focusing on active and passive reduction of structural vibrations have been designed to minimize the radiated noise within the aircraft cabin or cockpit. The type of sandwich considered in this paper is inspired from the trim panel, and consists of a relatively thick and lightweight honeycomb core bounded on the sides by two thin - but sufficiently stiff - sheets (homogeneous layer or laminates). For instance, the use of piezoelectric patches or constrained viscoelastic layers increase the structure's stiffness and damping. These methods are efficient but imply non-negligible additional mass. In the helicopter industry, trim panel core cells are filled out with small elements, such as empty elastomer spheres. They are embedded in a way that prevents a granular effect. They increase the damping at a reduced mass cost. The starting point of this study is to select the core cells that will be filled out instead of filling all the cells. The idea is to create a network of heterogeneities within the panel that will modify the structural wave propagation.

On one side, many studies on structural irregularities (manufacturing defaults or modifications made on purpose) have shown specific and interesting features. Most of the time, these irregularities are arranged following periodic patterns, as for instance in an aircraft with the ribs and stringers of fuselage frames.[2] Initially, a frequency shift of the density of states (abbreviated DOS) has been observed in proteins[3] between classical - unlocalized - modes called *phonons* and localized *fracton* modes, caused by energy localization phenomena. One-dimensional coupled mechanical oscillator studies[4] have highlighted such confinement, both experimentally and numerically. Rao *et al.*[5] studied large amplitude flexural vibration of stiffened plates. They used a finite element method to solved a non-linear equation and compared the first six modes natural frequencies with other studies of the same test-cases. However, he did not investigate the overloading influence on the mode shape or on higher order modes. Recently, studies have been conducted on fractal overloaded structures, specifically string[6] and membrane.[7] Experimental and numerical mode shapes exhibited *fractons* with spatial localization of the transverse displacement, which has been validated by a DOS analysis.

On the other side, acoustical aspects of architectured materials † have also been investigated. The present study follows on from a patent by ONERA and ATECA of 2015.[9] Indeed, they performed acoustic transmission experiments on sandwich panels whose cores were heterogeneously overloaded. Some honeycomb core cells were filled out by hollowed spheres (made of rigid polymer or damped elastomer), and the distribution patterns followed Vicsek and Sierpinski fractals. The experimental data suggested that the fractal distributions not only added lumped mass but also acted as a network of heterogeneities modifying the wave propagation among the structure and thus the acoustic radiated noise. However, no measurement of mechanical behavior of the overloaded structures or modeling have been performed.

Furthermore, phononic (or sonic) crystals exhibit frequency band gaps or wave-guiding due to destructive interferences generated by multiple scattering and wave reflections. Phononic crystal is a larger family that encompasses vibration in crystal lattices and phonon physics.[10] These structures are built by embedding a periodic array of scatterers in a host medium, either solid or fluid. Studies[11] comparing classically ordered networks with quasi-ordered fractal networks demonstrated that by removing some scatterers, the attenua-

†. This terminology is used by many, as for instance Hasby.[8] It is also referred as "hierarchical materials".

tion band gaps can be broadened and dropped to lower frequencies. Nouh *et al.* proposed meta-structures, as beams[12] and plates.[13] They were made of aluminum which were drilled to create multiple holes, filled with a viscoelastic membrane, surmounted by small masses. These local resonators acted as absorbers that dropped the band gaps towards lower frequencies, which cannot be reached only with the periodicity of the structure. The propagation surfaces were simulated by studying an elementary cell and considering the plate as infinite, ignoring the boundary conditions. Band gaps occurred and they achieved reduction of the structural vibrations in these bands. However, their structures suffered from a loss in the mechanical strength, due to the manufacturing process.

To summarize, the spatial localization of vibration mode shapes due to the periodic or pseudo-periodic overloading of structures has been modeled and experimentally studied, as well as the resulting acoustic radiation but for different purposes and in separate studies. However, to the best of the authors' knowledge, they do not account for the vibroacoustical coupling, neither on composite sandwich structures, nor with the heterogeneities directly inserted within the honeycomb core and following a fractal distribution. Such study has been performed by Derré and Simon[14] in a one-dimensional structure : a beam. The results are encouraging, both from a structural and an acoustical point of view. To be applied to an industrial construction, the structural model has to be extended to two-dimensional case : a sandwich plate.
This is the purpose of the present paper, organized as follows. Section 2 describes the mechanical model of a homogenized sandwich panel. A discrete eigenvalue problem is established and solved through a matrix formulation. Then, section 3 validates the structural model by a comparison with theoretical analytic results. Section 4 introduces the fractal overloading and discusses the numerical simulations of the aforementioned model, overloaded by the mass fractal distribution. Finally, some concluding remarks are drawn and an outlook of the acoustical possibilities is presented.

2. HOMOGENIZED PLATE MODEL

The first section presents the mechanical model of a non-overloaded sandwich panel, governed by bending dynamics. First, the homogenization of the material is described. Then, the simply-supported case is fully derived, with a time-harmonic motion equation and a finite differences approximation.

A. COMPOSITE HOMOGENIZATION

A typical sandwich trim panel consists of a lightweight core material trapped between two laminates, with several plies of glass-fiber. Herein, the core is made of Nomex®. The purpose of such a core is to maintain distance between the laminates and, to some extent resist to shear deformation.[15] In the modeling of acoustic radiation created by mechanical vibration (fluid-structure interaction), bending waves have a predominant role in the sound frequency domain.[1]

Considering Nilsson's simplifying assumptions,[16] a low-frequency equivalent bending rigidity of the whole structure can be derived using Huygens theorem (transport of the second moment of area from the neutral line of a skin to neutral line of the sandwich structure). For this kind of honeycomb core, there are two privileged bending directions L and W, linked to orthotropy due to its geometry and construction process. Most of the time, these directions influence the sandwich layout within the system in order to maximize their effects. In order to simplify the notations, the L and W directions are taken arbitrarily following the x and y directions. The equivalent bending rigidities in the $x-$direction D^L_{sand} and in the $y-$direction D^W_{sand} (also written D_x and D_y) are given by Eq. (1), where E_i, I_i, and h_i, respectively denote Young's moduli, second moments of area (of the cross section), and the thickness of elements. The indexing (c) and (s) are for the core and skin values. The skins are assumed to be made of an isotropic material. Kim and Hwang[17]

examined the validity conditions of the approximation used in such a model. The bending rigidity of the skins projected to the neutral line of the sandwich is predominant. The thickness $(h_c + h_s)$ confers to the ensemble a large equivalent bending stiffness, called sandwich effect. In the rest of the paper, the structure is considered as an orthotropic equivalent material with the bending rigidities approximated by Eq. (1).

$$\left\{\begin{array}{rcl} D^L_{\text{sand}} & = & E^L_c I_c + E_s I_s = E^L_c \dfrac{h_c^3}{12} + 2\,E_s \left(\dfrac{h_s^3}{12} + h_s \left(\dfrac{h_c + h_s}{2}\right)^2\right), \\ D^W_{\text{sand}} & = & E^W_c I_c + E_s I_s = E^W_c \dfrac{h_c^3}{12} + 2\,E_s \left(\dfrac{h_s^3}{12} + h_s \left(\dfrac{h_c + h_s}{2}\right)^2\right). \end{array}\right. \tag{1}$$

B. SIMPLE BENDING PLATE EQUATION

Under the classical linear hypotheses and approximations,[1] a fourth-order theory is used. Considering a thin Kirchhoff-Love plate, the time-dependency is taken as harmonic, with the corresponding angular frequency ω. The out-of-plane transverse displacement $u_z(x, y)$ of the time-dependent plate transverse displacement $u(x, y, t) = u_z(x, y) \times \exp(j\omega t)$ governs the equation of motion (2)

$$\Big(D\nabla^4 - \omega^2\rho h\Big) u_z(x, y) = \left(D_x \frac{\partial^4}{\partial x^4} + D_y \frac{\partial^4}{\partial y^4} + 2D_{xy} \frac{\partial^4}{\partial_x^2 \partial y^2} - \omega^2 \rho h\right) u_z(x, y) = 0\,, \tag{2}$$

with D, ρ, and h respectively denoting the generic term for bending rigidity (D_{xy} being the torsional rigidity), the density of the material, and the total plate thickness.

C. FINITE DIFFERENCES APPROXIMATION

In order to use finite differences (abbreviated FD) for the approximation of the spatial derivative operators, the structure has to be discretized. The FD method is mainly motivated by its convenience of implementation and a low computing-time cost. It is also justified by the flexibility of the structure meshing for the integration of heterogeneities at different fractal orders. Finally, it allows an easier understanding of the results from a physical point of view.

The structure is regularly discretized with $L_x = h_x \times (N_x + 1)$ and $L_y = h_y \times (N_y + 1)$, as sketched in Fig. 1. There are $N_{\text{pts}} = N_x \times N_y$ points inside the mesh as the exterior points, meaning the edge and corner points are considered fixed ($\times$ in Fig. 1). Indeed, the boundary conditions considered in the present study are simply-supported on all the edges (abbreviated SSSS). The total number of points is $(N_x + 2) \times (N_y + 2)$. The transverse displacement at position (i) is written as $u(i) = u_{(i)}$.

So, $u_z(x, y)$ becomes a discrete variable $u_{(i)}$ and the derivative operators can be approximated with FD. A centered second-order scheme is used for the fourth-order derivative. The x-direction is taken as reference to express the stencil support around a point $x_{(i)}$, which gives a classical thirteen points scheme - as sketched in Fig. 1. Eq. (2) can be recast into a discrete finite differences equation as

$$\begin{aligned} & u_{(i)} \left(6\frac{D_x}{h_x^4} + 6\frac{D_y}{h_y^4} + 8\frac{D_{xy}}{h_x^2 h_y^2} - \omega_n^2 \rho h\right) + \left(u_{(i\text{-}2)} \frac{D_x}{h_x^4} + u_{(i+2)} \frac{D_x}{h_x^4} + u_{(i\text{-}2N_x)} \frac{D_y}{h_y^4} + u_{(i+2N_x)} \frac{D_y}{h_y^4}\right) \\ & - 4\Big(u_{(i\text{-}1)} \left(\frac{D_x}{h_x^4} + \frac{D_{xy}}{h_x^2 h_y^2}\right) + u_{(i+1)} \left(\frac{D_x}{h_x^4} + \frac{D_{xy}}{h_x^2 h_y^2}\right) + u_{(i\text{-}N_x)} \left(\frac{D_y}{h_y^4} + \frac{D_{xy}}{h_x^2 h_y^2}\right) \\ & + u_{(i+N_x)} \left(\frac{D_y}{h_y^4} + \frac{D_{xy}}{h_x^2 h_y^2}\right)\Big) + 2\frac{D_{xy}}{h_x^2 h_y^2}\Big(u_{(i\text{-}N_x\text{-}1)} + u_{(i\text{-}N_x+1)} + u_{(i+N_x\text{-}1)} + u_{(i+N_x+1)}\Big) = 0\,, \end{aligned} \tag{3}$$

with ω_n the discrete pulsation. Indeed, due to the variable discretization, the number of degrees of freedom is equal to the size of the discrete displacement vector $u_{(i)}$, meaning N_{pts}.

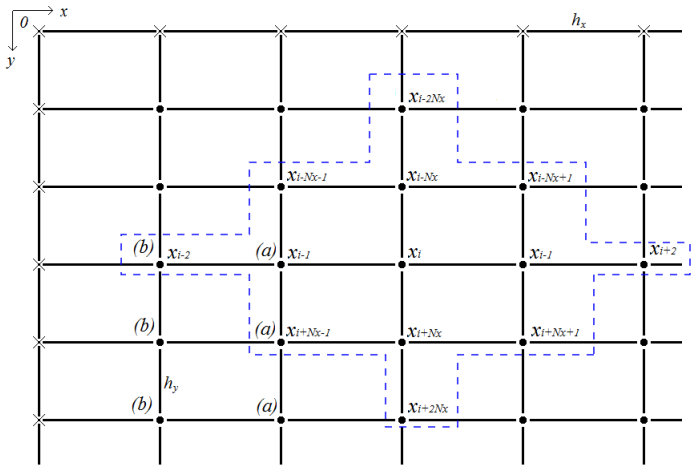

Fig. 1: Grid mesh with axis reference and 13 points stencil (– –) for the finite differences approximation.

D. MATRIX FORMULATION

The system created by the equations (3) for the N_{pts} discrete points $u_{(i)}$ is an eigenvalue problem, with N_{pts} unknowns. On the stencil sketch of Fig. 1, the choice of x as the main index leads to a formulation that can be easily recast into matrices. Each line of the mesh corresponds to set of (N_x) points represented in a (N_x)-by-(N_x) matrix. The global matrix is therefore a $(N_x \times N_y)$-by-$(N_x \times N_y)$ matrix. The time-dependency term $\left(-\omega_n^2\, \rho h\, u_{(i)}\right)$ is integrated separately at the end of this part in Eq. (9). For a point $u_{(i)}$ taken far enough from the boundaries, which are treated in the next section, five clusters of points are identified. A first group of five points ($u_{(i\text{-}2)}$, $u_{(i\text{-}1)}$, $u_{(i)}$, $u_{(i+1)}$, $u_{(i+2)}$) can be integrated within a (N_x)-by-(N_x) pentadiagonal matrix $[M_{\text{c}}]$ with the main expression being

$$[M_{\text{c}}] = \begin{bmatrix} 0 & \ddots & \ddots & \ddots & & \ddots & & \ddots & 0 & & \\ \cdots & 0 & \dfrac{D_x}{h_x^4} & -4\left(\dfrac{D_x}{h_x^4}+\dfrac{D_{xy}}{h_x^2h_y^2}\right) & \left(6\dfrac{D_x}{h_x^4}+6\dfrac{D_y}{h_y^4}+8\dfrac{D_{xy}}{h_x^2h_y^2}\right) & -4\left(\dfrac{D_x}{h_x^4}+\dfrac{D_{xy}}{h_x^2h_y^2}\right) & \dfrac{D_x}{h_x^4} & 0 & \cdots \\ & & 0 & \ddots & \ddots & \ddots & \ddots & \ddots & 0 & & \end{bmatrix} \tag{4}$$

The second and third groups are ($u_{(i\text{-}N_x\text{-}1)}$, $u_{(i\text{-}N_x)}$, $u_{(i\text{-}N_x\text{+}1)}$) and ($u_{(i+N_x\text{-}1)}$, $u_{(i+N_x)}$, $u_{(i+N_x\text{+}1)}$). They are identical because of their symmetry around the central term $u_{(i)}$. Their main expressions can be integrated into a (N_x)-by-(N_x) tridiagonal matrix $[M_{\text{m}}]$ as in Eq. (5). The fourth and fifth groups are ($u_{(i\text{-}2N_x)}$) and ($u_{(i+2N_x)}$). They are identical for the same reason and are composed of a single term on their diagonals $\left(D_y/h_y^4\right)$, which leads to (N_x)-by-(N_x) matrix $[M_{\text{ext}}]$, also presented in Eq. (5).

$$[M_{\text{m}}] = \begin{bmatrix} 0 & \ddots & \ddots & \ddots & 0 & & \\ \cdots & 0 & 2\dfrac{D_{xy}}{h_x^2h_y^2} & -4\left(\dfrac{D_x}{h_x^4}+\dfrac{D_{xy}}{h_x^2h_y^2}\right) & 2\dfrac{D_{xy}}{h_x^2h_y^2} & 0 & \cdots \\ & & 0 & \ddots & \ddots & \ddots & 0 \end{bmatrix}; [M_{\text{ext}}] = \begin{bmatrix} 0 & \ddots & 0 & & \\ \cdots & 0 & \dfrac{D_y}{h_y^4} & 0 & \cdots \\ & & 0 & \ddots & 0 \end{bmatrix} \tag{5}$$

The global assembly matrix $[M_{\text{ass}}]$ of the system can therefore be expressed as Eq. (6).

$$[M_{\text{ass}}] = \begin{bmatrix} & \ddots & \ddots & \ddots & \ddots & \ddots & & & \\ \cdots & [0] & [M_{\text{ext}}] & [M_{\text{m}}] & [M_{\text{c}}] & [M_{\text{m}}] & [M_{\text{ext}}] & [0] & \cdots \\ & & & \ddots & \ddots & \ddots & \ddots & \ddots & \end{bmatrix} \tag{6}$$

The boundary conditions need to be integrated and are modifying the firsts and lasts rows of these matrices.

E. BOUNDARY CONDITION INTEGRATION

In this part, the integration of one condition is presented into details. The others ones are integrated following the same approach. The panel is considered as SSSS on all of its edges. Therefore, the transverse displacements and the bending momentum are equally null on the extremities.[1] The momentum is approximated with a center FD scheme around a given position $x_{(j)}$, such as Eq. (7)

$$M_{xx} = D_x \frac{\partial^2 u}{\partial x^2} = \frac{D_x}{h_x^2} \left(u_{(j\text{-}1)} - 2u_{(j)} + u_{(j+1)} \right) . \tag{7}$$

When the global equilibrium Eq. (3) is evaluated along the $(x = 0)$ edge, it is equal to zero with $u_{(i)}$ null too. If the equation is evaluated on a position marked as (a) on Fig. 1, the point $u_{(i\text{-}2)}$ is an edge point, so it is equal to zero. That leads to the removing of the left term $\left(D_x/h_x^4\right)$ in the second row of the $[M_\text{c}]$ matrix of Eq. (4). If the equation is evaluated on a position marked as (b), the point $u_{(i\text{-}2)}$ is off-domain, and the points $u_{(i\text{-}1)}$, $u_{(i\text{-}N_x\text{-}1)}$ and $u_{(i+N_x\text{-}1)}$ are equal to zero because they are on the edge. If Eq. (7) is evaluated on an edge, it is equals to zero and the central term $u_{(j)}$ is null too. So, the first term $u_{(j\text{-}1)}$ is out of the plate physical domain, but through the equation it is therefore equal to the opposite of the last term $\left(u_{(j\text{-}1)} = -u_{(j+1)}\right)$. Thus, the previous relationship leads to $\left(u_{(i\text{-}2)} = -u_{(i)}\right)$, which substituted into the first row of the matrix (4) gives

$$[M_\text{c}] = \begin{bmatrix} \left(5\frac{D_x}{h_x^4}+6\frac{D_y}{h_y^4}+8\frac{D_{xy}}{h_x^2h_y^2}\right) & -4\left(\frac{D_x}{h_x^4}+\frac{D_{xy}}{h_x^2h_y^2}\right) & \frac{D_x}{h_x^4} & 0 & \cdots \\ -4\left(\frac{D_x}{h_x^4}+\frac{D_{xy}}{h_x^2h_y^2}\right) & \left(6\frac{D_x}{h_x^4}+6\frac{D_y}{h_y^4}+8\frac{D_{xy}}{h_x^2h_y^2}\right) & -4\left(\frac{D_x}{h_x^4}+\frac{D_{xy}}{h_x^2h_y^2}\right) & \frac{D_x}{h_x^4} & 0 \\ \ddots & \ddots & \ddots & \ddots & \ddots \end{bmatrix} \tag{8}$$

Due to the symmetry of the geometry, the same expressions as the first and second rows are found for the last and second to last rows respectively. The green six 6 of Eq. (8) corresponds to the derivative in the y-direction, and therefore is not modified for the point (a), a case in hand taken far from the top and bottom boundaries. The third and all the other rows are the five components rows of Eq. (4).
If the time-dependency term is reintroduced, the global matrix formulation of (6) is recast into Eq. (9)

$$\left(\left[M_\text{ass} \right] - \omega_n^2 \, \rho h \, \left[\mathbb{I}_{N_\text{pts}} \right] \right) (U) = \left(\Theta_{N_\text{pts}} \right) \tag{9}$$

with $\left[\mathbb{I}_{N_\text{pts}} \right]$ the identity matrix and $\left(\Theta_{N_\text{pts}} \right)$ the null-vector. The vector $(U) = \left(u_{(1)} \; ... \; u_{(N_x N_y)} \right)^T$ is the displacement vector of the $u_{(i)}$ degrees of freedom. Eq. (9) forms an eigenvalue problem, with the solutions of ω_n giving the natural frequencies and associated mode shapes.

3. VALIDATION FOR SIMPLY-SUPPORTED PANEL

This part presents the model validation for a SSSS plate. The model wavenumbers and mode shapes are compared with the theoretical results. The approximation precision is mainly related to the stencil size.

A. THEORETICAL SOLUTIONS

The analytic harmonic solutions of the transverse displacement (u^th) of a SSSS plate under simple bending dynamics are[1]

$$u^\text{th}(x,y) = \sum_{l=1}^{+\infty} \sum_{m=1}^{+\infty} a_{l,m} \, \phi_{l,m}(x,y) \qquad \text{with} \qquad \phi_{l,m}^\text{th}(x,y) = \sin\left(k_l^\text{th} \, x\right) \times \sin\left(k_m^\text{th} \, y\right) , \tag{10}$$

where $a_{l,m}$ is the amplitude of the mode (l,m), $\phi^{\text{th}}_{l,m}(x,y) = \phi^{\text{th}}_{l}(x) \times \phi^{\text{th}}_{m}(y)$ and $\left(k^{\text{th}}\right)^2 = \left(\left(k^{\text{th}}_{l}\right)^2 + \left(k^{\text{th}}_{l}\right)^2\right)$ of Eq. (10) being respectively the plate mode shape and the wavenumber. The rotation frequency is a function of the wavenumber as Eq. (11)

$$k^{\text{th}}_{l} = \frac{l\pi}{L_x}\,, \qquad k^{\text{th}}_{m} = \frac{m\pi}{L_y}\,, \qquad \text{and} \qquad \omega^{\text{th}} = \left(k^{\text{th}}\right)^2 \left(D/\rho h\right)^{1/2}. \tag{11}$$

B. WAVENUMBER

The panel is uniformly discretized in $(N_x = 180)$ and $(N_y = 162)$ elements in each direction, leading to $(h_x \simeq 5.6mm$ and $h_y \simeq 5.6mm)$ stencils, which lie in the standard honeycomb core cell size (for trim panels, the usual lengths of a core cell lie in the $[4.0\,;\,6.4]$mm range). Table 2 presents a comparison between the wavenumbers, with k^{th} theoretical values and k the FD model values.

$$\left\{ \text{Diff.} = |\, k^{\text{th}} - k\,|\,, \qquad \text{and} \qquad \text{Rel.} = \left(\frac{\text{Diff.}}{k^{\text{th}}}\right) \times 100\,. \right. \tag{12}$$

The first modes present good results, with small differences. Generally, when the mode order increases, the

Designation	L_x	L_y	h_c	h_s	h	ρ	E^L_c	E^W_c	E_s	N_x	N_y
Unit	(m)	(m)	(mm)	(mm)	(mm)	(kg.m^{-3})	(MPa)	(MPa)	(MPa)		
Value	1	0.9	9.56	0.42	10.4	264.4	1.25	0.73	625	180	162

Table 1: Quantities and values of the numerical simulations.

Mode	(1,1)	(1,2)	(2,1)	(2,2)	(18,4)	(28,1)
k^{th}	4.6962	7.1877	7.6556	9.3924	58.247	88.034
k	4.6951	7.1872	7.6513	9.3898	58.023	87.171

Table 2: Comparison between the model and theoretical wavenumbers.

discrepancies between the FD model and the theory increase too. If a higher-order mode is observed, for instance the mode (18,4), meaning approximately 19 points per wavelength, there is a relative difference of about 0.004%, which is acceptable. If a resolution limit of 13 points per wavelength is considered, it leads in the x-direction with $N_x = 180$ points to approximately fourteen wavelengths, meaning the mode 28 in that direction. If such a mode is evaluated, for instance the mode of order (28,1), there is a relative difference of about 0.01%, which is still acceptable. Even though the model slightly underestimates the wavenumbers, the theoretical and FD model values are in found to be in a very good agreement.

C. MODE SHAPE

The mode shapes are compared using the Modal Assurance Criterion (abbreviated MAC). The MAC is a measure of the degree of linearity[18] between two modes, estimated from their mode shapes. In the present paper, it is used to compare the theoretical and the FD mode shapes. The auto-MAC of FD mode shapes has been found to be identically equal to one on the diagonal and zero elsewhere, meaning the modes are perfectly orthogonal and the linear assumption is confirmed. The cross-MAC between the theoretical and

the FD values has also been calculated, and found with a diagonal of ones and zeros elsewhere. The modes are orthogonal and well identified, as previously. The simply-supported FD model is considered as validated compared to the theoretical values, in terms of wavenumbers and mode shapes.

4. OVERLOADED PANEL SIMULATIONS

This part presents how the heterogeneities are integrated within the structure and how they are modeled in the FD model. The fractal distribution is then presented. Finally, the influence of the overloads is analyzed through the simulations of fractal panels. The influence of the fractal mode shape is investigated, as well as the impact on the modal frequencies.

A. INTEGRATION OF AN OVERLOAD

If a honeycomb core panel is filled out with small heterogeneities, they add mass and damping within the structure. However, in the case where only a few core cells are filled in order to create a network of scatterers for the structural wave, the main effect is the added mass. Indeed, it is locally creating a mechanical impedance breakdown, due to the material differences (*e.g.* composition and density), giving rise to reflected and transmitted waves. A small part of the energy can also be dissipated locally, through material damping mechanism. This phenomena occurs mainly when the distance between the heterogeneities is proportional to half the structural wavelength, leading to wave interferences. If the point $x_{(k)}$ is overloaded with a mass M_{over} (in kg), Eq. (3) is modified into

$$\begin{aligned} u_{(k)}\left(6\frac{D_x}{h_x^4}+6\frac{D_y}{h_y^4}+8\frac{D_{xy}}{h_x^2h_y^2}-\omega_n^2\left(\rho h+\frac{M_{\text{over}}}{h_xh_y}\right)\right)+\left(u_{(k\text{-}2)}\frac{D_x}{h_x^4}+u_{(k+2)}\frac{D_x}{h_x^4}+u_{(k\text{-}2N_x)}\frac{D_y}{h_y^4}\right. \\ \left.+u_{(k+2N_x)}\frac{D_y}{h_y^4}\right)-4\Big(u_{(k\text{-}1)}\left(\frac{D_x}{h_x^4}+\frac{D_{xy}}{h_x^2h_y^2}\right)+u_{(k+1)}\left(\frac{D_x}{h_x^4}+\frac{D_{xy}}{h_x^2h_y^2}\right)+u_{(k\text{-}N_x)}\left(\frac{D_y}{h_y^4}+\frac{D_{xy}}{h_x^2h_y^2}\right) \\ \left.+u_{(k+N_x)}\left(\frac{D_y}{h_y^4}+\frac{D_{xy}}{h_x^2h_y^2}\right)\right)+2\frac{D_{xy}}{h_x^2h_y^2}\Big(u_{(k\text{-}N_x\text{-}1)}+u_{(k\text{-}N_x\text{+}1)}+u_{(k+N_x\text{-}1)}+u_{(k+N_x\text{+}1)}\Big)=0\,, \end{aligned} \tag{13}$$

with $\left(\frac{M_{\text{over}}}{h_xh_y}\right)$ being a surface density (in kg.m^{-2}). The local overloading mass ratio α_{loc} is defined as Eq. (14)

$$\alpha_{\text{loc}}=\frac{\rho h}{\left(\rho h+\frac{M_{\text{over}}}{h_xh_y}\right)}\,. \tag{14}$$

Eq. (13) can be expressed as $\frac{\alpha_{\text{loc}}}{\rho h}\Big(D\nabla^4 u\Big)=\omega_n^2\,u_{(k)}$, where the FD scheme is not expanded or recast into a matrix formulation like

$$\left(\frac{1}{\rho h}[\mathbb{I}_{k,\alpha_{\text{loc}}}]\,[M_{\text{ass}}]\,-\omega_n^2\left[\mathbb{I}_{N_{\text{pts}}}\right]\right)(U)=\left(\Theta_{N_{\text{pts}}}\right) \tag{15}$$

where $[\mathbb{I}_{k,\alpha_{\text{loc}}}]$ is the identity matrix, where the term of the k-line is replaced by (α_{loc}).

B. INTEGRATION OF FRACTAL OVERLOADED DISTRIBUTIONS

The term "fractal" † has been introduced by Mandelbrot in 1977.[19] It defines a infinite curve or surface generated by a self-similar pattern that repeats itself - or a part of itself - at different scales. A construction

†. inspired from the Latin word *fractus* that means broken or fractured.

generated by a finite number of iterations n^{frac} is called pre-fractal. In order to simplify the notation in this paper, the considered pre-fractals are called simply fractals or n^{frac}-order fractals.

The distributions used in this study are inspired from the Cantor set. Its iterative construction process for mono-dimensional structure has a homothetic ratio of three : at each iteration (order), the element is sub-divided into three equal parts. The first three orders are presented on the top of Fig. 2a, as well as the order zero, which is the initial structure. The distributions used are strongly inspired from this set, except that only the extremities of the sub-sets are marked and correspond to the local overloads, sketched by black dots (•) on the bottom of Fig. 2a. These are the patterns used for mono-dimensional structures as in previous

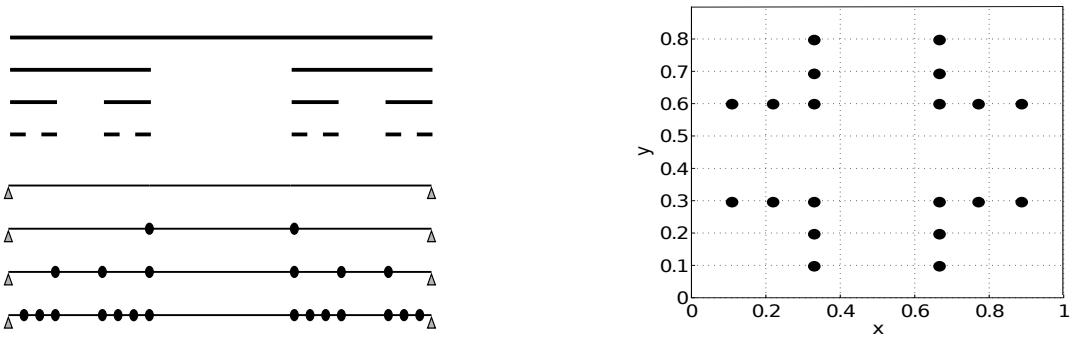

(a) Cantor set and overloaded beam. *(b) A (2-2) order fractal.*

Fig. 2: (a) Cantor set on the top and beams overloaded with fractal on the bottom, both from orders 0 up to 3, and (b) a (2-2) order fractal distribution on a panel, the (•) representing the punctual overloads.

studies,[7,14] which has been extended here for two-dimensional panels. Figure 2b presents for instance the example of a fractal of second-order both in the x-direction and in the y-direction, called (2-2) order fractal, in the case of a rectangular panel of size $1m \times 0.9m$, with the characteristics of Table 1. In the mono-dimensional case, the n_x^{frac}order fractal results in p_x masses calculated : $p_x = \sum_{i=1}^{n_x^{\text{frac}}} 2^i = 2 \times \left(2^{n_x^{\text{frac}}} - 1\right)$. The same relation can be used in the y-direction such as $p_y = 2 \times \left(2^{n_y^{\text{frac}}} - 1\right)$. The total number of masses p_{xy} for a two-dimensional structure as sketched on Fig. 2b is derived by combining these two relations and removing the first-order points which appear four times : $p_{xy} = 2p_x + 2p_y - 4 = 2 \times (p_x + p_y - 2)$. The p_{xy} overloads are integrated within the system using the same procedure as described in the previous section 4.1, leading to the multiplication of the associated matrix lines by (α_{loc}) of the matrix $[\mathbb{I}_{\alpha_{\text{loc}}}]$. For this study, each overload is assumed to have the same mass M_{over}. The global total overlaoding ratio α_{tot} is defined such as the ratio of overloaded fractal beam mass over the non-overloaded beam mass as Eq. (16)

$$\alpha_{\text{tot}} = \frac{(\rho h L_x L_y + p_{xy} \times M_{\text{over}})}{\rho h L_x L_y} = 1 + \frac{p_{xy} \times M_{\text{over}}}{\rho h L_x L_y} \,. \tag{16}$$

C. INFLUENCE OF THE FRACTAL ORDER

The plate characteristics are tabulated in Table 1. Table 3 sums up the overloading positions along a length normalized to the unity. The inter-mass distance of order 2 is about $a_2 = 1/9 \simeq 0.1111$ and of order 3 about $a_3 = 1/27 \simeq 0.037$. The mode (17,5) is studied in this paper because of its wavelengths. It presents sixteen nodes in the x-direction, if the extremities are not counted, and four in the y-direction. These nodes are separated by a distance of $\lambda_{17}/2 = 0.0588$m (or per cent in this case, as the length is equal to the unity). The nodes positions are listed in (17).

Position							
Frac. 2	/	/	0.1111	0.2222	/	/	0.3333
Frac. 3	0.0370	0.0741	0.1111	0.2222	0.2593	0.2963	0.3333
Frac. 2	0.6667	/	/	0.7778	0.8889	/	/
Frac. 3	0.6667	0.7040	0.7410	0.7778	0.8889	0.9260	0.9630

Table 3: Overloading positions in per cent along a direction for fractal orders 2 and 3.

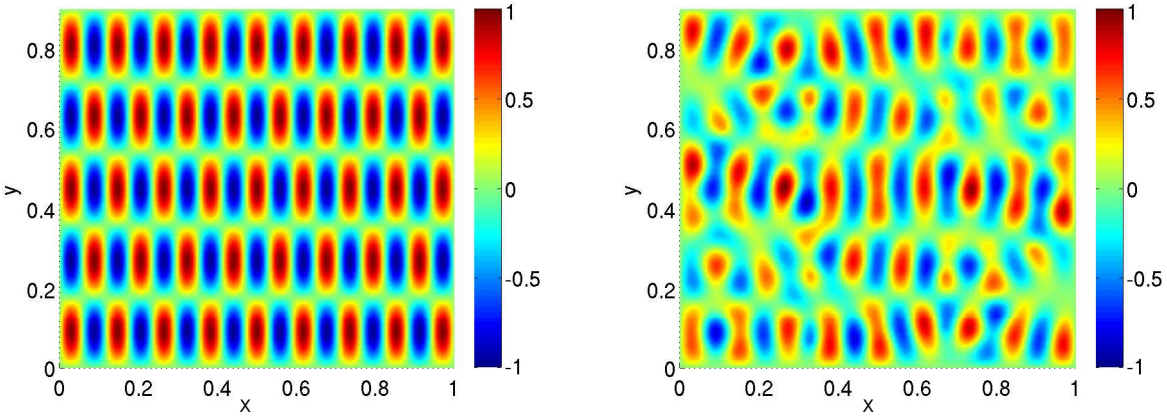

(a) Empty panel. ***(b) A (3-3) order panel.***

Fig. 3: (17,5) mode shapes of (a) an empty panel, and (b) a (3-3) fractal panel with $\alpha_{tot} = 1.0946$.

$$\text{Node positions : } \begin{array}{l} \{0.0588;\ 0.1176;\ 0.1765;\ 0.2325;\ 0.2941;\ 0.3333;\ 0.3529;\ 0.4118;\ldots \\ 0.5294;\ 0.5882;\ 0.6471;\ 0.7059;\ 0.7647;\ 0.8235;\ 0.8824;\ 0.9414\}\ . \end{array} \tag{17}$$

By comparing the node and mass positions, it can be seen that several nodes are very close to the overloads, both for order 2 and 3. That is why in this case the mode shapes are modified along the fractal distribution as in Fig. 3b. Indeed, as half the wavelength is comparable with the inter-mass distances, the bending waves are reflected and lead to destructive interferences. This is why the amplitudes are smaller. This phenomena occurs for all the multiples of half the wavelength. This phenomena will not happen if the masses are positioned perfectly on the nodes, because they will be considered as fixed and will only reduce the modal frequency due to the mass. The mode (17,5) has one of its node on a mass, but this is negligible. In the (2-2) fractal panel of Fig. 3b, it can clearly be seen that the two lines of masses in the x-direction (at $y = [0.3; 0.6]$) have shown reduced amplitudes in the laterals parts, whereas the amplitude in the mid-part is less affected.

As a comparison, the mode (18,6) is quickly presented in Fig. 4, with a non over-loaded panel and a fractal (2-2) one. There is barely no difference between the two mode shapes, even though some masses are not perfectly on nodes. These differences explain the small discrepancies between the mode shapes.

D. EVOLUTION OF THE MODAL FREQUENCIES

The Table 4.4 presents the frequencies of the mode (17,5) for different fractal orders and overloadings. As expected, the frequency decreases as the fractal order increasing, since the plate becomes heavier. To

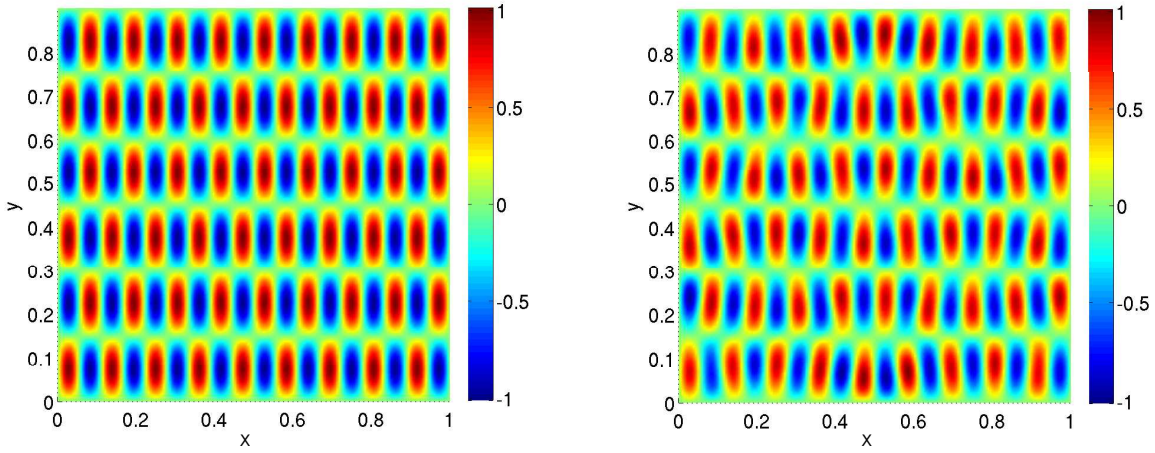

(a) Empty panel. *(b) A (2-2) order panel.*

Fig. 4: (18,6) mode shapes of (a) an empty panel, and (b) a (2-2) fractal panel with $\alpha_{tot} = 1.0202$.

be more precise, for a density increase of α_{tot}, the mode frequency is decreased by a factor $\left(\alpha_{\text{tot}}^{-1/2}\right)$, from Eq. (11). Indeed, the frequency ratio between a non-overloaded and a fractal panel can be written as Eq. (18)

$$\frac{f^{\text{frac}}}{f^{\text{non-o}}} = \frac{(k)^2 \left(\alpha_{\text{tot}} D/\rho h\right)^{1/2}}{(k)^2 \left(D/\rho h\right)^{1/2}} = \left(\alpha_{\text{tot}}^{-1/2}\right) . \tag{18}$$

The mode wavelength is assumed to be the same in both cases, only the amplitude is modified by the presence of the fractal, as it can be seen in Fig. 3 and 4. For instance, this frequency ratio between the non-overloaded panel and the (3-3) fractal panel with an overloading $(\alpha_{\text{tot}} = 1.0946)$ is $(1.0431/1.0923 = 0.95501)$, where the theoretical value is $(1.0946^{-1/2} = 0.9558)$. The relative errors between the theory and the FD model have been calculated and found to be very small, as shown in Table 4.4. Indeed, the largest relative difference is about 2.6% for this mode.

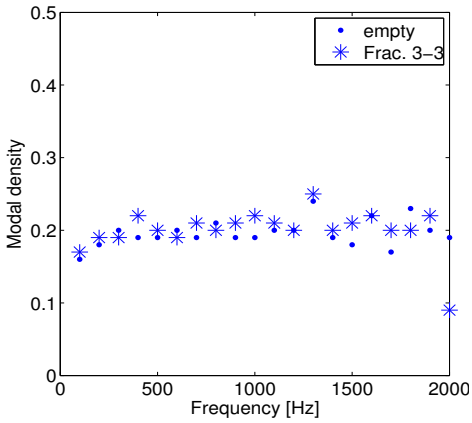

Fig. 5: Modal densities of the empty (•) and of the (3-3) fractal panels (∗).

Frac.	M_{over}	α_{loc}	α_{tot}	f (kHz)	Rel.
Empty	/	1	1	1.0923	/
(2-2)	0.0025	0.0325	1.0202	1.0747	1.12
(2-3)	0.0025	0.0325	1.0364	1.0650	1.62
(3-2)	0.0025	0.0325	1.0364	1.0621	1.89
(3-3)	0.0025	0.0325	1.0525	1.0565	2.04
(2-2)	0.0045	0.0183	1.0364	1.0621	1.89
(2-3)	0.0045	0.0183	1.0655	1.0513	2.21
(3-2)	0.0045	0.0183	1.0655	1.0476	2.56
(3-3)	0.0045	0.0183	1.0946	1.0431	2.32

Table 4: Overloading, fractal values for the mode (17,5).

The modal density of the plate is calculated by only taking into account the bending modes, as in the mechanical model. Under the hypothesis of a thin flat plate (wavelengths of the considered modes much

larger than the plate thickness), an approximation[1] of the modal density $n(\omega)$ is given by Eq. (19)

$$n(\omega) = \frac{dN_b}{d\omega} = \frac{L_x L_y}{4\pi} \left(\frac{\rho h}{D} \right)^{1/2} , \tag{19}$$

with N_b the mode-count function. It can be observed that the theoretical modal density of dispersive bending waves is constant and independent of the frequency. Figure 5 presents the modal density of the non-overloaded panel and of the (3-3) fractal panel, with overloading $\alpha_{\text{tot}} = 1.0946$. The mean modal density of the 400 first modes are 0.196 mode per Hz for the non-overloaded beam and 0.2 for the fractal beam. The modal densities are not perfectly constant but still present a vertical asymptote. As the increase of density is α_{tot}, the modal density is increased by a factor $\alpha_{\text{tot}}^{1/2}$, from Eq. (19). The theoretical increase can be calculated with Eq. (20) as the ratio of modal densities of the fractal panel over the non-overloaded panel.

$$n^{\text{frac}}/n^{\text{non-o}} = \left(\alpha_{\text{tot}}^{1/2} \right) . \tag{20}$$

In this case study, it is equal to 1.0462. The numerical increase equals $(0.2/0.196 \simeq 1.0204)$. The relative error between the theory and the FD model is $(1.0462 - 1.0204)/1.0462 = 2.47\%$. From the previous result, the model is able to predict the variation of the modal density.

5. CONCLUSION

The effects of a fractal distribution of masses on the mechanical behavior of sandwich plates have been studied in this paper. The composite structure is modeled as a homogenized material under simple bending dynamics, then discretized and approximated by a finite difference method. Heterogeneities are integrated within the material as additional masses distributed following a Cantor-like set. The eigenvalue problem is finally solved numerically to obtain the *in vacuo* modal basis. The non-overloaded model has been validated with a comparison to the analytic results for simply-supported boundary conditions. Simulations of fractally overloaded panels exhibit localization phenomena when the inter-mass distance is comparable to half the structural wavelength. It has been demonstrated that half the wavelength needs to be close to this dimension but not exactly equal, otherwise the masses are on the nodes and therefore do not modify the mode shapes. The fractal order has been investigated and the higher is the fractal mode, the strongest is the localization. The increase of the modal density is observed and well predicted based on the mass increase.

Future work will include computing of the acoustic radiation of such a structure, as is already done in the mono-dimensional case[14] for a beam. The current implementation is already valid for these calculations, as the radiation efficiency can be computed using a radiation resistance matrix[1] obtained from the transverse displacements of the structure discretized in elementary radiators. Indeed, the finite difference discretization provides elements which fulfill the hypotheses in terms of size compared to the wavelength. An extension of the finite differences model will include a more advanced modeling of the composite dynamics, to improve the precision of the mode shape and frequency, especially at higher frequencies. It would therefore take into account the shear effects, and the coupling between the transverse and torsional displacements.

The major benefit of the presented paper is its ability to intrinsically model and simulate the bending dynamics of overloaded structures, with a reduced cost-time, compared to finite element methods for instance, in terms of time and memory consumption. The mode shape reduction and localization due to the fractal pattern show encouraging results for the acoustical radiation, with its application to the aerospace industry.

ACKNOWLEDGMENTS

This research has been supported jointly by the Midi-Pyrénées region and ONERA.

REFERENCES

[1] F. Fahy and P. Gardonio, *Sound and structural vibration - Radiation, Transmission and Response*, second edition, Academic Press, Elsevier, 2007.

[2] D. J. Mead, "Wave propagation in continuous periodic structures : research contributions from Southampton 1964-1995.", *Journal of Sound and Vibration*, Vol. 190, No. 3, 1996, pp. 495–524.

[3] S. Alexander and R. Orbach, "Density of states on fractals : "fractons".", *Journal de Physique Lettres*, Vol. 43, No. 17, 1982, pp. 625–631.

[4] C. H. Hodges and J. Woodhouse, "Vibration isolation from irregularity in a nearly periodic structure : Theory and measurements.", *The Journal of the Acoustical Society of America*, Vol. 74, No. 3, 1983.

[5] S. R. Rao, A. H. Sheikh, and M. Mukhopadhyay, "Large-amplitude finite element flexural vibration of plates/stiffened plates." *The Journal of the Acoustical Society of America*, Vol. 93, No. 3, 1993.

[6] E. Bertaud du Chazaud, D. Chareryon, and V. Gibiat, "Elastic waves in 2D self-similar structures : localisation, vibrational integrated density of state and distribution of the scatterers.", *Proceedings of the 4th acoustical European meeting Forum Acusticum*, Budapest, June 2005.

[7] E. Bertaud du Chazaud and V. Gibiat, "A numerical study of 1D self-similar waveguides : Relationship between localization, integrated density of states and the distributions of the scatterers.", *Journal of Sound and Vibration*, Vol. 313, No. 3-5, 2008, pp. 631–642.

[8] M. Hasby, "Designing architectured materials.", *Scripta Materialia*, Vol. 68, No. 1, 2013, pp. 4–7.

[9] ONERA / ATECA, "Soundproof panel", *Patent* WO 2015/117868 A1, Bulletin of 13.08.2015.

[10] M. I. Hussein, M. J. Leamy, and M. Ruzzene, "Dynamics of Phononic Materials and Structures : Historical Origins, Recent Progress, and Future Outlook.", *Applied Mechanics Reviews*, Vol. 66, No. 4, 2014, pp. 040802–040802-38.

[11] J. V. Sánchez-Pérez, V. Romero-García, L. M. Garcia-Raffi, and S. Castiñeira-Ibáñez, "Improved attenuation bands using quasi-fractal structures.", *Proceedings of EURONOISE 2009*, Edinburgh, Oct. 2009.

[12] M. Nouh, O. Aldraihem, and A. Baz, "Vibration characteristics of metamaterial beams with periodic local resonances.", *Journal of Vibration and Acoustics*, Vol. 136, No. 6, 2014, pp. 061012–061012-12.

[13] M. Nouh, O. Aldraihem, and A. Baz, "Wave propagation in metamaterial plates with periodic local resonances.", *Journal of Sound and Vibration*, Vol. 341, 2015, pp. 53–73.

[14] J. Derré and F. Simon, "Concept of "fractal" helicopter trim panel.", *Proceedings of ERF 2016, 42nd European Rotorcraft Forum*, Lille, Sep. 2016.

[15] D. Backström and A. C. Nilsson, " Modelling the vibration of sandwich beams using frequency dependent parameters.", *Journal of Sound and Vibration*, Vol. 300, No. 3-5, 2007, pp. 589–611.

[16] A. C. Nilsson, "Wave propagation in and sound transmission through sandwich plates.", *Journal of Sound and Vibration*, Vol. 138, No. 1, 1990, pp. 73–94.

[17] H.-Y. Kim and W. Hwang, "Effect of debonding on natural frequencies and frequency response functions of honeycomb sandwich beams.", *Composite Structures*, Vol. 55, No. 1, 2002, pp. 51–62.

[18] R. J. Allemang, "The Modal Assurance Criterion Twenty Years of Use and Abuse.", *Sound and vibration*, Vol. 37, No. 8, 2003, pp. 14–23.

[19] B. B. Mandelbrot, *Fractals : Form, Chance, and Dimension*, first edition, Mathematics Series, W. H. Freeman, 1977.